Interplay between bulk and edge-bound topological defects in a square micromagnet

Sam D. Sloetjes, Einar Digernes, Fredrik K. Olsen, Rajesh V. Chopdekar, Scott T. Retterer, Erik Folven, and Jostein K. Grepstad

Citation: Appl. Phys. Lett. **112**, 042401 (2018);
View online: https://doi.org/10.1063/1.5010166
View Table of Contents: http://aip.scitation.org/toc/apl/112/4
Published by the American Institute of Physics

Interplay between bulk and edge-bound topological defects in a square micromagnet

Sam D. Sloetjes,[1] Einar Digernes,[1] Fredrik K. Olsen,[1] Rajesh V. Chopdekar,[2,3] Scott T. Retterer,[4] Erik Folven,[1] and Jostein K. Grepstad[1]
[1]*Department of Electronic Systems, Norwegian University of Science and Technology, NO-7491 Trondheim, Norway*
[2]*Swiss Light Source, Paul Scherrer Institute, CH-5232 Villigen PSI, Switzerland*
[3]*Department of Materials Science and Engineering, University of California, Davis, California 95616, USA*
[4]*Center for Nanophase Materials Sciences, Oak Ridge National Laboratory, Oak Ridge, Tennessee 37831, USA*

(Received 23 October 2017; accepted 8 January 2018; published online 22 January 2018)

A field-driven transformation of a domain pattern in a square micromagnet, defined in a thin film of $La_{0.7}Sr_{0.3}MnO_3$, is discussed in terms of creation and annihilation of bulk vortices and edge-bound topological defects with half-integer winding numbers. The evolution of the domain pattern was mapped with soft x-ray photoemission electron microscopy and magnetic force microscopy. Micromagnetic modeling, permitting detailed analysis of the spin texture, accurately reproduces the measured domain state transformation. The simulations also helped stipulate the energy barriers associated with the creation and annihilation of the topological charges and thus to assess the stability of the domain states in this magnetic microstructure. https://doi.org/10.1063/1.5010166

Detailed knowledge of domain state transformations in patterned thin film micromagnets is important to their implementation in spintronic devices. Numerous studies over the past two decades have focused on static domain patterns in different geometries[1–4] and field-driven transitions between different domain states.[5–9] It was shown that such transitions are often associated with formation and displacement of magnetic objects such as vortices, antivortices, and domain walls (DWs).

Adopting a framework of topological defects is helpful when discussing such complex spin textures.[10–16] For example, by introducing topological defects, one-dimensional DWs in thin film nano- and micromagnets can be effectively reduced to zero-dimensional point defects,[17–19] thus reducing the complexity of the analysis. Bulk topological defects are central to a number of recent experimental studies of magnetic nanosystems, notably in work discussing vortex dynamics,[20–24] but also in static experiments.[25–27] The latter typically consider the possibility to control either vortex core polarization or vortex chirality. A recent study by Wintz *et al.*[28] demonstrates how a gyrating vortex may serve as a tunable spin-wave emitter. Topological edge defects, introduced by Tchernyshyov and Chern to analyze complex spin textures in flat nanomagnets,[29] were successfully invoked to explain DW motion in nanowire geometries.[16,30] However, experimental evidence for the behavior of such edge defects in thin film nano- and micromagnets is scarce.[13]

In this work, we investigate in detail the interplay between bulk and edge topological defects in a field-driven domain transformation in a thin film micromagnet. Our model system is a $2\,\mu m \times 2\,\mu m$ square ferromagnet defined in a $La_{0.7}Sr_{0.3}MnO_3$ (LSMO) epilayer and embedded in a nonmagnetic matrix. Using soft x-ray photoemission electron microscopy (X-PEEM) and magnetic force microscopy (MFM), we monitor the transition from a flux-closure ground state of this micromagnet to a remanent domain state with a high net magnetization and explain this finding by topological constraints. Micromagnetic simulations are in keeping with the experimental findings and help estimate the energy barriers associated with nucleation and annihilation of the topological defects.

Thin film micromagnets typically feature a demagnetization field that forces in-plane orientation of a majority of the magnetic moments, which effectively results in a spin texture of the same universality class as the XY-model. Topological defects in such spin structures are associated with spatial circulation of the moments around any arbitrary point[18] and can be described in terms of a winding number defined as $n = \frac{1}{2\pi}\oint_{\partial\Omega} \nabla\theta \cdot d\mathbf{r}$,[17,29] which measures the change in spin angle θ when tracing a path around the defect core. A prominent example is the vortex, in which the moments rotate in the same direction as the increasing angle when encircling the vortex core. This defect has a winding number $n = +1$. A defect with the moments turning in the opposite direction of the integration path is referred to as an anti-vortex and has a winding number $n = -1$.

Besides topological defects with an integer winding number in the interior of a 2D spin lattice, referred to as bulk defects, additional defects with a fractional winding number may exist at the micromagnet boundaries. Their winding numbers are calculated as $n = \frac{1}{2\pi}\int_{\partial\Omega} \nabla(\theta - \theta_\tau) \cdot d\mathbf{r} = \pm 1/2$.[29] Here, θ_τ denotes the spin orientation with respect to the edge. Fractional defects can be considered as integer defects cut in half by the boundary. The total winding number, or "charge" n, is always conserved according to the Poincaré-Hopf theorem in topology[16,18]

$$n_{total} = \sum_i^{bulk} n_i + \sum_i^{edge} n_i = 1 - g, \tag{1}$$

where g is the number of "holes" (i.e., non-magnetic regions) inside the sample.

Samples with 2 μm × 2 μm square micromagnets embedded in a nonmagnetic matrix were prepared by e-beam lithography and Ar^+ ion implantation of 100 u.c. (40 nm) LSMO thin films grown epitaxially with pulsed laser deposition on (001)-oriented 0.05 wt. % Nb-doped $SrTiO_3$ (Nb:STO) substrates. At these lateral dimensions, the micromagnets are at the border of an expected transition from Landau flux-closure to more complicated domain states.[3] The LSMO growth conditions and the patterning process were reported in earlier work.[31–33] Atomic force micrographs revealed step-and-terrace growth, and x-ray diffraction showed that the films were fully strained to the substrate. The squares were aligned with their edges along the ⟨110⟩ crystalline directions, i.e., the magnetocrystalline easy axes of LSMO.

Magnetic measurements were carried out with X-PEEM on the Surface/Interface Microscopy (SIM) beamline at the Swiss Light Source (SLS).[34] Ferromagnetic domain contrast was obtained from magnetic circular dichroism at the Mn L_3 absorption edge. The left/right-handed circularly polarized x-rays were incident at a 16° grazing angle with the in-plane projection oriented along edges of the square micromagnets. The magnetic domain images were recorded at approximately 225 K, which is well below the Curie temperature of our LSMO films. X-PEEM measurements with an *in situ* applied magnetic field are notoriously difficult, as the field will deflect the photoemitted electrons, thus distorting the recorded image. However, the X-PEEM set-up at SLS allows small magnetic fields up to 2.5 mT during imaging by tilting the sample to compensate for the deflection of the emitted electrons. This tilt results in fewer electrons reaching the detector, however, and thus in an impaired image quality.

In the absence of an applied magnetic field, the ferromagnetic squares display the familiar Landau flux-closure domain state shown in Fig. 1(a), characterized by four triangular domains forming a vortex at their common apex in the center of the square. A small stationary magnetic field of 2.5 mT imposed along the (horizontal) square diagonal increases the extent of the two bottom triangular domains, both with a magnetization component in the direction of the applied field, at the expense of the two domains at the top corner of the micromagnet, see Fig. 1(b). When a field pulse of 50 mT is applied to this sample (i.e., prior to the measurement), the Landau flux-closure is replaced by a magnetic domain state resembling the letter Z, cf. Fig. 1(c), hereafter referred to as the "Z-domain." In the literature, a similar domain state has been referred to as either an "S-domain"[8,35] or a "C-domain."[4] This domain pattern was previously found in an antiferromagnetic/ferromagnetic $LaFeO_3$/LSMO bilayer system and explained in terms of an exchange bias sufficient to drive the square micromagnet into a remanent state with finite overall magnetization.[36] Our X-PEEM data show that this Z-domain persists in remanence also for an LSMO single-layer micromagnet. A field pulse of 50 mT applied in the opposite direction produces a stable Z-domain with opposite magnetization, cf. Fig. 1(d).

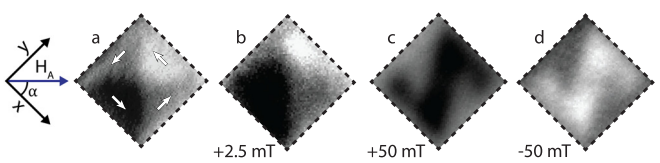

FIG. 1. Experimental observation of magnetic domain state transitions in a 2 μm × 2 μm square LSMO micromagnet. (a) Landau flux-closure, (b) with shifted position of the vortex core in a field of +2.5 mT applied along the (horizontal) square diagonal, (c) Z-domain in remanence after a field pulse of +50 mT, and (d) Z-domain with opposite net magnetization after a field pulse of −50 mT.

In the following, we discuss the details of this domain state transition within a framework of topological defects, relying on 2D micromagnetic simulations using the software package MuMax3[37] with magnetic parameters typical of LSMO, i.e., exchange stiffness $A_{ex} = 1.7\,\mathrm{pJ/m}$ and saturation magnetization $M_S = 400\,\mathrm{kA/m}$.[38,39] The biaxial anisotropy constant was set to $K_1 = 4\,\mathrm{kJ/m^3}$.[40] The simulated magnetic structure, with dimensions corresponding to those of our thin film squares, was partitioned into cells with lateral dimensions smaller than the magnetostatic exchange length, $l_S = \sqrt{2A_{ex}/(\mu_0 M_S^2)} = 4.11\,\mathrm{nm}$. Hence, the in-plane cell size was set to 2 nm × 2 nm, with the out-of-plane cell dimension equal to the film thickness.

MuMax3 solves the Landau-Lifshitz-Gilbert equation. We assume that the applied field rises slowly ($\tau_H > 10^{-6}$ s) compared to the timescale characteristic of spin dynamics ($\tau_s < 10^{-8}$ s), i.e., the magnetic domain state transition is modeled as a quasi-static process. The field was increased in increments of ∼0.01 mT with in-field relaxation of the magnetization after each increment. This strategy allows the magnetic moments sufficient time to settle in a minimum energy state throughout the simulation.

When a small external field is applied along the square diagonal ($\alpha = 45°$) [Fig. 2], the simulated magnetic domain pattern resembles that observed experimentally [Fig. 1(b)]. This is a distorted flux-closure domain state [Fig. 2(a)] with the $n = +1$ vortex defect moving along the square diagonal perpendicular to the direction of the applied field [Fig. 2(b)]. At a threshold field strength of approximately 7 mT, pairs of fractionally charged topological defects appear at diagonally opposite corners of the square with the two defects in each pair having opposite charges ($n = \pm 1/2$). The $n = -1/2$ defects move rapidly along the edges towards the top corner [Fig. 2(c)] coming to a halt as they approach the $n = +1$ vortex defect, whereas the $n = +1/2$ topological defects stay put at their respective corners. The halted motion of the $n = -1/2$ edge defects was found to be contingent upon a sufficiently large magnetocrystalline anisotropy. If a biaxial anisotropy constant of $K_1 \ll 4\,\mathrm{kJ/m^3}$ is used in this simulation, such as that representative of metallic ferromagnets like permalloy, the $n = -1/2$ defects will not come to a halt, but will directly annihilate with the $n = +1$ bulk topological defect at the top corner. The magnetocrystalline anisotropy appears to introduce an energy barrier, which impedes rotation of the spins that constitute the edge defects and thus halts the continued motion of these defects towards the top corner.

When the applied field is increased beyond some critical value, the $n = +1$ vortex core defect and the two $n = -1/2$ edge defects annihilate [Fig. 2(d)], leaving only the two $n = +1/2$ edge defects at diagonally opposite corners of the square. Thus, the overall topological charge is conserved throughout the three stages of this field-imposed domain

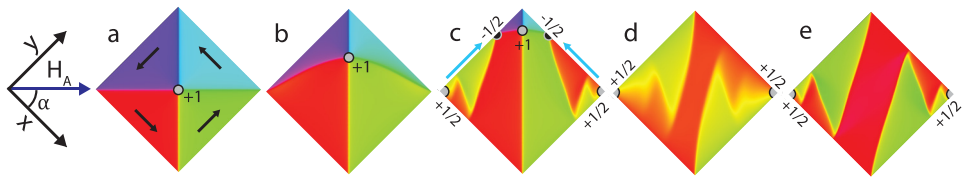

FIG. 2. Characteristic domain states of a 2 μm × 2 μm micromagnet with topological defects indicated. (a) Landau flux-closure in the absence of an applied field, (b) with a displaced vortex core for an applied field of 5 mT, (c) after creation of fractional edge defects in an applied field of 7 mT, (d) after annihilation of the $n = +1$ core defect and the two $n = -1/2$ edge defects in an applied field >14 mT (light green and red colors indicate magnetic moments with orientation between red and green), and (e) domain state in remanence after removal of the applied field.

state transformation from the Landau flux-closure to the Z-domain, in accordance with the Poincaré-Hopf theorem [Eq. (1)]. If the applied field is removed prior to annihilation of the $n = +1$ and the two $n = -1/2$ defects, the domain pattern of the 2 μm × 2 μm square will revert to the Landau flux-closure. However, once annihilated the Z-domain persists in remanence with a net magnetization of $m_x = 0.6\,M_S$, $m_y = 0.4\,M_S$ [Fig. 2(e)]. This domain state obtained in simulations closely matches that observed in X-PEEM for the square LSMO micromagnets [Figs. 1(c) and 1(d)].

The events of creation and annihilation of topological defects are accompanied by concomitant "jumps" in the virgin magnetization curve, as shown in Fig. 3. The first jump at 7 mT marks the threshold field for creation of the edge defects, after which the defects move rapidly about 3/4 the length of the edge towards the upper corner. If the applied field is reduced after this jump, the edge defects gradually move back towards the corners where they first emerged. This behavior is reflected in the smooth decline of the yellow remanent branch in Fig. 3. The kink on this branch at 4 mT coincides with the annihilation of the edge defects and restoration of the Landau flux-closure. The second jump at 14 mT is associated with annihilation of the $n = +1$ bulk defect and the two $n = -1/2$ edge defects, which serves to stabilize the Z-domain. The remanent nature of the Z-domain appears from the red branch, which shows a high net magnetization when the field is reduced to 0 mT.

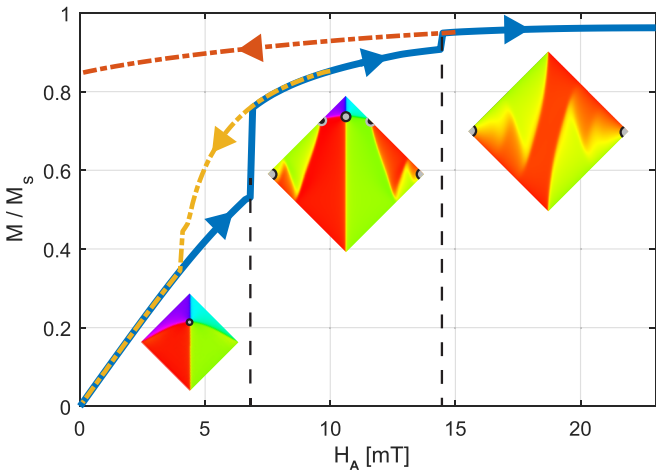

FIG. 3. The virgin magnetization curve (solid blue line) for the domain state transformation from Landau flux-closure to the Z-domain for an applied field H_A along the square diagonal. The jump in magnetization at 7 mT marks the creation of the fractionally charged edge defects depicted in Fig. 2(c), whereas the jump at approximately 14 mT marks the subsequent annihilation of the $n = +1$ and the two $n = -1/2$ defects, after which the Z-domain is stabilized. Additionally, hysteretic branches (dashed curves) are plotted from applied fields of 10 mT (yellow) and 15 mT (red).

The stable Z-domain in remanence suggests an energy barrier associated with restoration of the Landau flux-closure. The size of this energy barrier can be estimated by introducing a different kind of topological charge, the skyrmion charge q, which is related to the winding number n by $q = np/2$, where p denotes the polarization, i.e., the out-of-plane direction of the magnetic moment at the defect core.[10,41,42] Thus, the $n = +1$ vortex core defect carries a skyrmion charge of $q = +1/2$, whereas the $n = \pm 1/2$ edge defects carry no skyrmion charge since they have zero out-of-plane magnetic moment.[13] We note that the transition from the Z-domain to the Landau flux-closure involves the creation of a bulk vortex carrying a skyrmion charge of $q = 1/2$. The exchange energy of a skyrmion texture can be calculated as $E = 8\pi qAt$,[10,42] where A is the exchange stiffness and t denotes the film thickness. In our case, this corresponds to an energy $E = 4.7$ eV. This value is in close agreement with simulation results for the drop in exchange energy upon annihilation of the vortex core $(n = +1)$ and the two $n = -1/2$ edge defects. However, it should be noted that other energy contributions, such as the demagnetization energy, are not taken into account in this analysis. Locally, the demagnetization energy will be lowered by the formation of a vortex core. Thus, 4.7 eV places an upper bound on the magnitude of the energy barrier to recreation of the bulk vortex required for the transition from the Z-domain to Landau flux-closure.

In order to examine experimentally the intermediate domain state predicted by simulations, we also performed MFM measurements using an *attoAFM/MFM I* microscope. In this microscope, an atomically sharp and magnetized tip is scanned across the thin film surface to pick up the out-of-plane stray fields from the sample and thus is sensitive primarily to spin textures such as domain walls and defects. Moreover, MFM permits imaging in the presence of applied fields much higher than those possible with X-PEEM. The MFM measurements recorded at T = 5 K are summarized in Fig. 4. They show domain patterns in excellent agreement with those found in simulations [Figs. 2(a)–2(e)]. Imaging of the Z-domain in remanence proved to be difficult with MFM due to the strong sample-tip interaction. This interaction caused the domain state to switch during imaging in zero applied field. However, in a small field of 3 mT, the Z-domain was sufficiently stable to allow MFM imaging, cf. Fig. 4(e). In order to ascertain that the Z-domain is truly a remanent state, we also tested if it would persist without this external applied field. The MFM tip was retracted from the sample, and the field was switched off. A 3 mT external field was then switched back on,

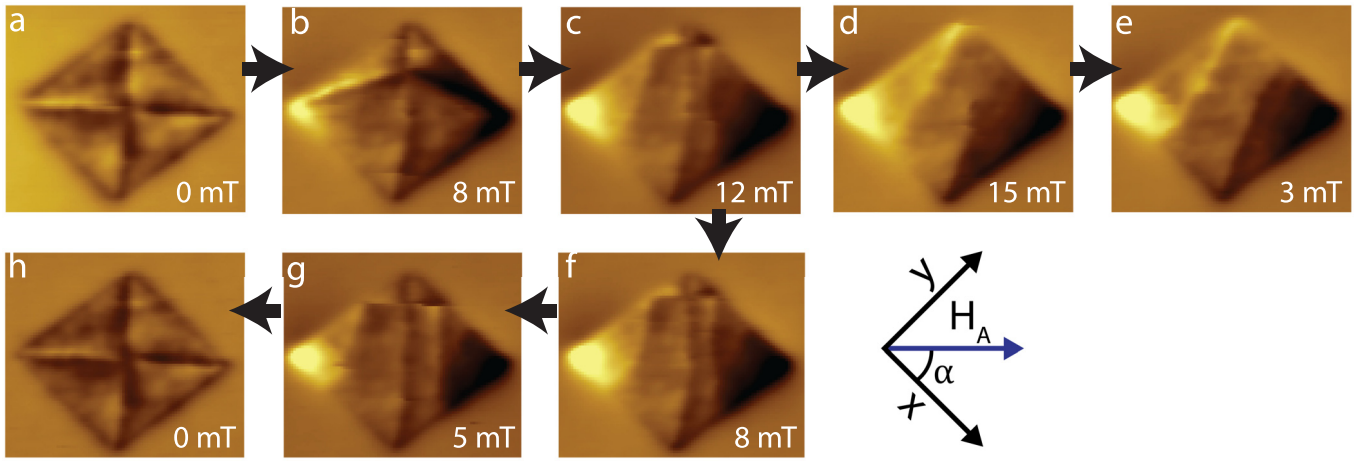

FIG. 4. MFM measurement of the magnetic domain state transitions in a 2 μm × 2 μm LSMO square platelet, with the easy axes oriented along the square's edges. (a) Landau flux-closure, (b) with a displaced vortex core for an applied field of 8 mT, (c) after creation of fractional edge defects in an applied field of 12 mT, (d) after annihilation of the $n = +1$ vortex core defect and the two $n = -1/2$ edge defects at an applied field >12 mT, and (e) Z-domain state imaged in a small stabilizing field of 3 mT. When the field is reduced before annihilation of the defects, the $n = -1/2$ edge defects can be seen to move back towards their respective nucleation sites, cf. (f) and (g), before the domain pattern eventually reverts to the Landau flux-closure (h).

followed by MFM imaging of the magnetic domain pattern. This measurement indeed demonstrates persistence of the Z-domain in remanence in agreement with the observed X-PEEM domain patterns in Figs. 1(c) and 1(d) and the micromagnetic simulation in Fig. 2(e). The micrographs displayed in Figs. 4(f)–4(h) show the behavior of the domain pattern when the field is lowered, corresponding to the dashed yellow curve in Fig. 3. These data display the same hysteretic behavior as that found in the micromagnetic simulations. At 5 mT [Fig. 4(g)], the edge defects are still present, thereby indicating a gradual retreat of the defects back to their corners of origin.

In summary, we report on a field-driven magnetic domain state transition in a 2 μm × 2 μm thin film LSMO micromagnet, investigated with X-PEEM and MFM. Analysis using micromagnetic simulations demonstrates that this transition from the Landau ground state to a remanent domain pattern with finite magnetization (the Z-domain) can be understood in terms of creation of topological edge defects and their interplay with a topological bulk defect (the flux-closure vortex core). We argue that the Z-domain is stabilized by the presence of an energy barrier associated with the difference in the skyrmion number between this domain state and the Landau flux-closure. The present work demonstrates how topological defects may be invoked to understand and describe micromagnetic domain state transitions and to assess their stability in remanence. This insight may open for new approaches to control the switching properties of micro- and nanomagnets.

Part of this work was performed on the Surface/Interface Microscopy (SIM) beamline of the Swiss Light Source, Paul-Scherrer-Institut in Villigen, Switzerland. We thank Dr. Armin Kleibert for helpful assistance with the X-PEEM measurements. We would also like to thank Jacob Linder, Johannes Skaar, and Gereon Quick for stimulating discussions. Partial funding for this work was obtained from the Norwegian Ph.D. Network on Nanotechnology for Microsystems, which is sponsored by the Research Council of Norway, Division for Science, under Contract No. 221860/F60.

[1]D. Goll, G. Schütz, and H. Kronmüller, Phys. Rev. B **67**(9), 094414 (2003).
[2]R. Hertel, Z. Metallkd. **93**(10), 957–962 (2002).
[3]L. Heyderman, S. Czekaj, F. Nolting, E. Müller, P. Fischer, P. Gasser, and L. Lopez-Diaz, J. Appl. Phys. **99**(6), 063904 (2006).
[4]J. Rhensius, C. Vaz, A. Bisig, S. Schweitzer, J. Heidler, H. Körner, A. Locatelli, M. Nino, M. Weigand, and L. Méchin, Appl. Phys. Lett. **99**(6), 062508 (2011).
[5]R. Escobar, N. Vargas, S. Castillo-Sepúlveda, S. Allende, D. Altbir, and J. d'Albuquerque e Castro, Appl. Phys. Lett. **104**(12), 123102 (2014).
[6]C. König, M. Sperlich, R. Heinesch, R. Calarco, J. O. Hauch, U. Rüdiger, G. Güntherodt, S. Kirsch, B. Özyilmaz, and A. D. Kent, Appl. Phys. Lett. **79**(22), 3648–3650 (2001).
[7]K. Kirk, M. Scheinfein, J. Chapman, S. McVitie, M. Gillies, B. Ward, and J. Tennant, J. Phys. D: Appl. Phys. **34**(2), 160 (2001).
[8]S. Cherifi, R. Hertel, J. Kirschner, H. Wang, R. Belkhou, A. Locatelli, S. Heun, A. Pavlovska, and E. Bauer, J. Appl. Phys. **98**(4), 043901 (2005).
[9]R. Cowburn, D. Koltsov, A. Adeyeye, M. Welland, and D. Tricker, Phys. Rev. Lett. **83**(5), 1042 (1999).
[10]A. A. Belavin and A. M. Polyakov, Pis'ma Zh. Eksp. Teor. Fiz. **22**, 503 (1975) [JETP Lett. **22**, 245 (1975)].
[11]S.-K. Kim, K.-S. Lee, Y.-S. Yu, and Y.-S. Choi, Appl. Phys. Lett. **92**(2), 022509 (2008).
[12]S. Bohlens, B. Krüger, A. Drews, M. Bolte, G. Meier, and D. Pfannkuche, Appl. Phys. Lett. **93**(14), 142508 (2008).
[13]K.-S. Lee, M.-W. Yoo, Y.-S. Choi, and S.-K. Kim, Phys. Rev. Lett. **106**(14), 147201 (2011).
[14]M. B. Jalil and S. G. Tan, Sci. Rep. **4**, 5123 (2014).
[15]O. Tretiakov and A. Abanov, J. Magn. Magn. Mater. **383**, 65–68 (2015).
[16]A. Pushp, T. Phung, C. Rettner, B. P. Hughes, S.-H. Yang, L. Thomas, and S. S. P. Parkin, Nat. Phys. **9**(8), 505–511 (2013).
[17]P. M. Chaikin and T. C. Lubensky, *Principles of Condensed Matter Physics* (Cambridge University Press, 2000), Vol. 1.
[18]N. D. Mermin, Rev. Mod. Phys. **51**(3), 591–648 (1979).
[19]B. Krüger and M. Kläui, "Topological defects in nanostructures—Chiral domain walls and skyrmions," in *Topological Structures in Ferroic Materials* (Springer, 2016), pp. 199–218.
[20]M. Bolte, G. Meier, B. Krüger, A. Drews, R. Eiselt, L. Bocklage, S. Bohlens, T. Tyliszczak, A. Vansteenkiste, B. Van Waeyenberge, K. W. Chou, A. Puzic, and H. Stoll, Phys. Rev. Lett. **100**(17), 176601 (2008).
[21]T. Kamionka, M. Martens, K. W. Chou, M. Curcic, A. Drews, G. Schütz, T. Tyliszczak, H. Stoll, B. Van Waeyenberge, and G. Meier, Phys. Rev. Lett. **105**(13), 137204 (2010).
[22]K. Y. Guslienko, X. F. Han, D. J. Keavney, R. Divan, and S. D. Bader, Phys. Rev. Lett. **96**(6), 067205 (2006).

[23]H. Jung, Y.-S. Yu, K.-S. Lee, M.-Y. Im, P. Fischer, L. Bocklage, A. Vogel, M. Bolte, G. Meier, and S.-K. Kim, Appl. Phys. Lett. **97**(22), 222502 (2010).
[24]B. Van Waeyenberge, A. Puzic, H. Stoll, K. W. Chou, T. Tyliszczak, R. Hertel, M. Fahnle, H. Bruckl, K. Rott, G. Reiss, I. Neudecker, D. Weiss, C. H. Back, and G. Schutz, Nature **444**(7118), 461–464 (2006).
[25]A. Lara, O. V. Dobrovolskiy, J. L. Prieto, M. Huth, and F. G. Aliev, Appl. Phys. Lett. **105**(18), 182402 (2014).
[26]J. Li, A. Tan, K. Moon, A. Doran, M. Marcus, A. Young, E. Arenholz, S. Ma, R. Yang, and C. Hwang, Appl. Phys. Lett. **104**(26), 262409 (2014).
[27]J. Pulecio, S. Pollard, P. Warnicke, D. Arena, and Y. Zhu, Appl. Phys. Lett. **105**(13), 132403 (2014).
[28]S. Wintz, V. Tiberkevich, M. Weigand, J. Raabe, J. Lindner, A. Erbe, A. Slavin, and J. Fassbender, Nat. Nanotechnol. **11**, 948–953 (2016).
[29]O. Tchernyshyov and G.-W. Chern, Phys. Rev. Lett. **95**(19), 197204 (2005).
[30]L. Thomas, M. Hayashi, R. Moriya, C. Rettner, and S. Parkin, Nat. Commun. **3**, 810 (2012).
[31]E. Folven, T. Tybell, A. Scholl, A. Young, S. T. Retterer, Y. Takamura, and J. K. Grepstad, Nano Lett. **10**(11), 4578–4583 (2010).
[32]E. Folven, A. Scholl, A. Young, S. T. Retterer, J. E. Boschker, T. Tybell, Y. Takamura, and J. K. Grepstad, Nano Lett. **12**(5), 2386–2390 (2012).
[33]Y. Takamura, R. V. Chopdekar, A. Scholl, A. Doran, J. A. Liddle, B. Harteneck, and Y. Suzuki, Nano Lett. **6**(6), 1287–1291 (2006).
[34]L. Le Guyader, A. Kleibert, A. F. Rodríguez, S. El Moussaoui, A. Balan, M. Buzzi, J. Raabe, and F. Nolting, J. Electron Spectrosc. Relat. Phenom. **185**(10), 371–380 (2012).
[35]H. Kronmüller, D. Goll, R. Hertel, and G. Schütz, Physica B **343**, 229–235 (2004).
[36]Y. Takamura, E. Folven, J. B. R. Shu, K. R. Lukes, B. Li, A. Scholl, A. T. Young, S. T. Retterer, T. Tybell, and J. K. Grepstad, Phys. Rev. Lett. **111**(10), 107201 (2013).
[37]A. Vansteenkiste, J. Leliaert, M. Dvornik, M. Helsen, F. Garcia-Sanchez, and B. Van Waeyenberge, AIP Adv. **4**(10), 107133 (2014).
[38]E. J. Kim, J. L. R. Watts, B. Harteneck, A. Scholl, A. Young, A. Doran, and Y. Suzuki, J. Appl. Phys. **109**(7), 07D712 (2011).
[39]T. Nagai, H. Yamada, M. Konoto, T. Arima, M. Kawasaki, K. Kimoto, Y. Matsui, and Y. Tokura, Phys. Rev. B **78**(18), 180414 (2008).
[40]M. S. Lee, T. A. Wynn, E. Folven, R. V. Chopdekar, A. Scholl, A. T. Young, S. T. Retterer, J. K. Grepstad, and Y. Takamura, ACS Nano **10**(9), 8545–8551 (2016).
[41]T. H. R. Skyrme, "Particle states of a quantized meson field," Proc. R. Soc. London, Ser. A **262**(1309), 237–245 (1961).
[42]O. A. Tretiakov and O. Tchernyshyov, Phys. Rev. B **75**(1), 012408 (2007).